Available online at www.sciencedirect.com
ScienceDirect
International Journal of Heat and Fluid Flow 29 (2008) 721–732
International Journal of HEAT AND FLUID FLOW
www.elsevier.com/locate/ijhff

# Direct and large eddy simulations of a bottom Ekman layer under an external stratification

John R. Taylor, Sutanu Sarkar *

*Department of Mechanical and Aerospace Engineering, University of California, San Diego La Jolla, CA 92093, United States*

Received 5 November 2007; received in revised form 18 January 2008; accepted 24 January 2008
Available online 2 April 2008

**Abstract**

A steady Ekman layer with a thermally stratified outer flow and an adiabatic boundary condition at the lower wall is studied using direct numerical simulation (DNS) and large eddy simulation (LES). An initially linear temperature profile is mixed by turbulence near the wall, and a stable thermocline forms above the mixed layer. The thickness of the mixed layer is reduced by the outer layer stratification. Observations from the DNS are used to evaluate the performance of the LES model and to examine the resolution requirements. A resolved LES and a near-wall model LES (NWM–LES) both compare reasonably well with the DNS when the thermal field is treated as a passive scalar. When buoyancy effects are included, the LES mean velocity and temperature profiles also agree well with the DNS. However, the NWM–LES does not sufficiently account for the overturning scales responsible for entrainment at the top of the mixed layer. As a result, the turbulent heat flux and the rate of change of the mixed layer temperature are significantly underestimated in the NWM–LES. In order to accurately simulate the boundary layer growth, the motions responsible for entrainment must either be resolved or more accurately represented in improved subgrid-scale models.


*Keywords:* Turbulence; Large eddy simulation; Geophysical boundary layer

## 1. Introduction

An externally stratified boundary layer forms when a fluid with a stable density stratification flows over an adiabatic surface. This situation is nearly ubiquitous at the bottom of the ocean where the seafloor can be approximated by an adiabatic condition (with the exception of isolated hydro-thermal hotspots). When the flow is unstratified, the height of a fully-developed rotating boundary layer, or Ekman layer, scales with $\delta = u^*/f$ where $u^*$ is the friction velocity and $f$ is the Coriolis parameter. Typically in the ocean $\delta = O(100\,\mathrm{m})$, but the observed boundary layer thickness is often $O(10\,\mathrm{m})$. This implies that the thickness of the oceanic bottom boundary layer is limited by the outer layer stratification.

In the atmosphere, a near-neutral (or conventionally-stable) boundary layer occurs when the heat flux at the surface is negligible and the boundary layer height is limited by a stable density inversion. This commonly occurs over the ocean where the surface heat flux tends to be smaller than over land (Businger and Charnock, 1983). Based on field observations and simulation results, Grant (1992) found that in the lower portion of a near-neutral atmospheric boundary layer, the dominant balance in the turbulent kinetic energy budget is formed between the production and dissipation, while away from the wall, the turbulent transport terms are non-negligible. Zilitinkevich and Esau (2003) used an LES to simulate the formation of a turbulent Ekman layer with an external stratification and vertical shear, both with and without a surface heat flux. They used their results to formulate a semi-empirical theory for the scaling of the boundary layer height.

Taylor et al. (2005) considered open channel flow with a stabilizing heat flux applied at the free surface and an

* Corresponding author.
*E-mail address:* sarkar@ucsd.edu (S. Sarkar).

0142-727X/$ - see front matter © 2008 Elsevier Inc. All rights reserved.
doi:10.1016/j.ijheatfluidflow.2008.01.017

adiabatic lower wall. With these boundary conditions, a well-mixed turbulent region formed near the lower wall and a region of stable stratification formed near the free surface. When the surface heat flux was large, the density difference between the lower mixed layer and the free surface was sufficient to inhibit upwelling of fluid from the mixed layer to the free surface. The primary effect of stratification was to limit the turbulent transport away from the wall relative to that observed in the unstratified case, and the vertical Froude number was identified as a useful parameter.

When a stabilizing heat flux exists at the boundary, as is often the case in nocturnal boundary layers (Mahrt, 1999), the effect of stratification is fundamentally different from an externally stratified boundary layer. Armenio and Sarkar (2002) used a LES to study stratified channel flow with a fixed temperature difference across the channel. Owing to the choice of boundary conditions, a heat flux was present near the wall which acted to limit the near-wall turbulent production. The authors found that simulations using a dynamic mixed model were able to accurately capture the effects of stratification on the bulk flow. In particular, the turbulent Prandtl number increased with the local gradient Richardson number as expected from previous laboratory and numerical studies. A stratified Ekman layer with a stabilizing heat flux applied at the lower boundary was studied using DNS by Coleman et al. (1992) and Shingai and Kawamura (2002). They found that the surface heat flux decreases the boundary layer height and increases the angle of the surface stress.

The goal of the present study is to use numerical simulations to examine the properties of an externally stratified Ekman layer with a particular emphasis on the thermal properties of the boundary layer. Since the role of stratification in the near-neutral case is significantly different from that in a stable boundary layer with a heat flux at the boundary, we have conducted a DNS in order to evaluate the performance of a resolved LES at the same Reynolds number. Once confidence in the LES model has been achieved through comparison with the DNS dataset, the resolution requirements can be examined by considering a low resolution NWM–LES. An accurate NWM–LES will allow simulations at a larger Reynolds number that is more appropriate for geophysical applications.

## 2. Formulation

A schematic of a bottom Ekman layer is shown in Fig. 1. Flow in the outer layer is assumed to be in geostrophic balance with a pressure gradient in the $y$-direction. The outer layer flow will therefore be aligned with the $x$-axis. The flow is bounded from below by a flat, no-slip, adiabatic surface, and periodic boundary conditions are applied in the horizontal directions. Near the wall, as molecular and turbulent viscosity affects the momentum balance, the flow turns in the direction of the pressure gradient, forming an Ekman spiral. Unlike a non-rotating boundary layer, the thickness of an Ekman layer is bounded and scales with

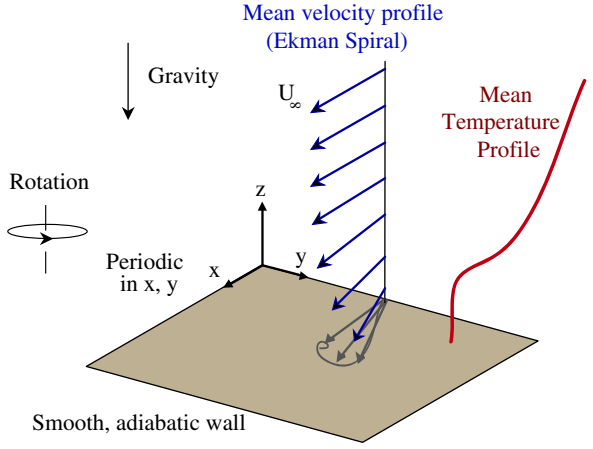


Fig. 1. Schematic: Benthic Ekman layer.

$\delta = u^*/f$ when the flow is not stratified. This is an advantage computationally since it is possible to set the domain size to be larger than the boundary layer height, and the boundary layer achieves a statistically steady state. When the outer layer flow is stratified, the boundary layer height will be further limited by the influence of stratification. An open boundary condition is applied at the top of the computational domain using a combination of a radiation condition and a Rayleigh damping region (Klemp and Durran, 1983). The boundary condition on the velocity field at the top of the computational domain is $\partial u_i/\partial z = 0$. This open boundary treatment has been shown to be effective in allowing turbulence-generated internal waves to freely leave the computational domain (Taylor and Sarkar, 2007a).

### 2.1. Governing equations

Using the friction velocity, $u^*$, the turbulent Ekman layer depth, $\delta = u^*/f$, and the outer layer temperature gradient, $\mathrm{d}\theta/\mathrm{dz}|_\infty$, the non-dimensional, spatially filtered governing equations can be written:

$$\frac{\partial \overline{\mathbf{u}}}{\partial t} + \overline{\mathbf{u}} \cdot \nabla \overline{\mathbf{u}} = -\frac{1}{\rho_0}\nabla \overline{p'} + f\widehat{\mathbf{k}} \times (U_\infty \widehat{\mathbf{i}} - \overline{\mathbf{u}}) - Ri_* \overline{\theta'}\widehat{\mathbf{k}} + \frac{1}{Re_*}\nabla^2 \overline{\mathbf{u}} - \nabla \cdot \boldsymbol{\tau}, \tag{1}$$

$$\frac{\partial \overline{\theta'}}{\partial t} + \overline{\mathbf{u}} \cdot \nabla \overline{\theta'} = \frac{1}{Re_* Pr}\nabla^2 \overline{\theta'} - \nabla \cdot \boldsymbol{\lambda}, \tag{2}$$

$$\nabla \cdot \overline{\mathbf{u}} = 0, \tag{3}$$

where

$$Re_* = \frac{u_* \delta}{\nu}, \quad Ri_* = \alpha g \frac{\mathrm{d}\theta}{\mathrm{dz}}|_\infty \frac{\delta^2}{u_*^2} = \frac{N_\infty^2}{f^2}, \quad Pr = \frac{\nu}{\kappa}, \tag{4}$$

$u^*$ is the friction velocity, $\nu$ is the molecular kinematic viscosity, $\kappa$ is the molecular diffusivity, $N_\infty$ is the outer layer buoyancy frequency, and $\boldsymbol{\tau}$ and $\boldsymbol{\lambda}$ are the subgrid-scale stress and density flux, respectively. The parameters con-

Table 1
Simulation parameters

| Type | $Re^*$ | $Ri^*$ | $(L_x,L_y,L_z)$ | $(N_x,N_y,N_z)$ | $min(\Delta_z^+)$ | $\Delta_x^+ = \Delta_y^+$ |
|---|---|---|---|---|---|---|
| DNS | 960 | 0, 1000 | $(2\delta, 2\delta, 2.7\delta)$ | (192,192,192) | 1.4 | 10 |
| Resolved LES | 960 | 0, 1000 | $(2\delta, 2\delta, 3\delta)$ | (96,96,96) | 1.8 | 20 |
| NWM–LES | 960 | 0, 1000 | $(2\delta, 2\delta, 3\delta)$ | (48,48,48) | 19.2 | 40 |

sidered in this study are listed in Table 1. Density changes are assumed to be caused by temperature variation in water, motivating the choice of Prandtl number, $Pr = 5$.

## 3. Numerical method

Simulations have been performed using an algorithm described in detail in Bewely et al. (2007). Since periodic boundary conditions are applied in the horizontal directions, derivatives in these directions are treated with a pseudo-spectral method, while derivatives in the vertical direction are computed with second-order finite differences. The low storage third-order Runge–Kutta–Wray method is Smagorinsky model was used by for time-stepping and viscous terms are treated implicitly with the Crank–Nicolson method. It can be shown that the numerical scheme ensures the discrete conservation of mass, momentum and energy (Bewely et al., 1999). In order to prevent spurious aliasing due to non-linear interactions between wavenumbers, the largest 1/3 of the horizontal wavenumbers are truncated using the 2/3 de-aliasing rule (Orszag, 1971). The vertical resolution of the direct numerical simulation is shown in Fig. 2 and compared to the Kolmogorov scale. The grid spacing is less than three times the Kolmogorov scale which should be sufficient for an accurate DNS (Moin and Mahesh, 1998).

The subgrid-scale stress tensor, $\boldsymbol{\tau}$ in Eq. (1) is evaluated using the dynamic mixed model (Zang et al., 1993; Vreman et al., 1997), and a dynamic eddy diffusivity model is used for the subgrid-scale heat flux, $\boldsymbol{\lambda}$:

$$\tau_{ij} = -2C\overline{\Delta}^2|\overline{\mathbf{S}}|\overline{S_{ij}} + \widehat{\overline{u_i}\overline{u_j}} - \widehat{\overline{u}}_i\widehat{\overline{u}}_j \tag{5}$$

and

$$\lambda_j = -2C_\theta\overline{\Delta}^2|\overline{\mathbf{S}}|\frac{\partial\overline{\theta}}{\partial x_j}. \tag{6}$$

The Smagorinsky coefficients, $C$ and $C_\theta$ are evaluated using the dynamic procedure. This is useful since it avoids an empirical specification of the Smagorinsky coefficient and has been shown to perform well for wall-bounded and density stratified flows (Armenio and Sarkar, 2002). The coefficients are evaluated by applying a test filter to the resolved velocity field and using the resolved fields and the test-filtered fields together to estimate the subgrid-scale stress and buoyancy flux. Specifically

$$C = \frac{M_{ij}L_{ij} - M_{ij}H_{ij}}{M_{kl}M_{kl}}, \tag{7}$$

where

$$L_{ij} = \widehat{\overline{u_i}\overline{u_j}} - \widehat{\overline{u}}_i\widehat{\overline{u}}_j, \quad M_{ij} = 2\overline{\Delta}^2|\overline{\mathbf{S}}|\widehat{\overline{S_{ij}}} - 2\widehat{\overline{\Delta}}^2\widehat{|\overline{\mathbf{S}}|}\widehat{\overline{S_{ij}}}, \tag{8}$$

$$H_{ij} = \widehat{\widehat{\overline{u}}_i\widehat{\overline{u}}_j} - \widehat{\overline{u}}_i\widehat{\overline{u}}_j - \left(\widehat{\overline{\overline{u}_i\overline{u}_j}} - \widehat{\overline{u}}_i\widehat{\overline{u}}_j\right), \tag{9}$$

and

$$C_\theta = \frac{M_i^\theta L_i^\theta}{M_j^\theta M_j^\theta}, \tag{10}$$

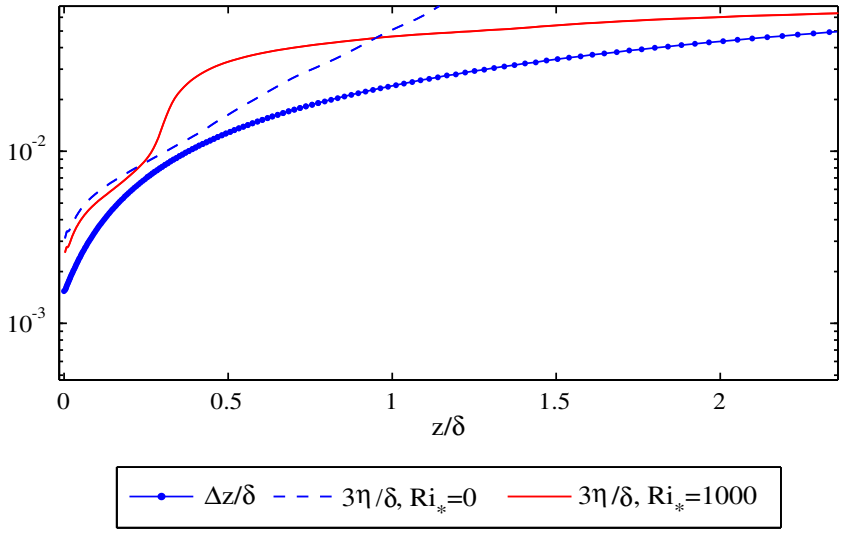


Fig. 2. Vertical grid spacing from the direct numerical simulations compared to $3\eta$ where $\eta$ is the Kolmogorov scale.

where

$$L_i^\theta = \widehat{\overline{\theta}\overline{u_i}} - \widehat{\overline{\theta}}\widehat{\overline{u_i}}, \quad M_i^\theta = 2\overline{\Delta}^2 \widehat{|\overline{\mathbf{S}}|\frac{\partial\overline{\theta}}{\partial x_i}} - 2\widehat{\overline{\Delta}}^2 \widehat{|\overline{\mathbf{S}}|}\frac{\widehat{\partial\overline{\theta}}}{\partial x_i}, \tag{11}$$

The test filter, denoted by $\widehat{\cdot}$, is applied over the horizontal directions only using the trapezoidal rule with a five-point stencil.

A *resolved* LES is usually defined as a simulation that resolves at least 80% of the energy everywhere in the flow (Pope, 2000). Near solid boundaries, turbulent motions scale with the viscous scale, $\delta_v = \nu/u^*$. Away from boundaries, the largest turbulent eddies are constrained by the domain size, $h$. Therefore, the ratio of the filter size near the wall to that necessary in the outer layer scales with $\delta_v/h = \nu/(u^* h) = 1/Re^*$. Even when considering a stretched grid in the wall-normal direction, this places a strong constraint on the grid spacing for resolved LES of wall-bounded flows at large Reynolds numbers.

In order to ease the grid resolution requirement and allow simulations at a large Reynolds number, it is possible to use a near-wall model in conjunction with the LES. The model that we have used is a modification of that proposed by Schumann (1975), Grotzbach (1987), and Piomelli et al. (1989), and modified slightly for a rotating boundary layer. This model uses an approximate boundary condition for the horizontal velocity near the wall by predicting the wall stress. Since a staggered grid is used in the vertical direction, the wall location is made coincident with the streamwise stress and the vertical velocity. The first horizontal velocity point away from the wall is located at $z^+(1) = 9.8$ in wall units, and the near-wall grid spacing is $\Delta z^+(1) = 19.2$. The first gridpoint is nearer to the wall than is common practice for near-wall models, and represents a tradeoff between near-wall grid spacing and resolution in the stratified boundary layer. If a grid spacing of $40^+$ wall units were used, there would only be five gridpoints between the wall and the top of the stratified boundary layer at $z = 0.2\delta$. We have found that the location of the first gridpoint does not affect the ability of the NWM–LES to capture the expected log-law. Once the grid is determined, the plane average of the streamwise velocity at the first point away from the wall is used to estimate the friction velocity by iteratively solving the expected mean logarithmic law:

$$\frac{\langle|\mathbf{u}|\rangle(1)}{u_*} = \frac{1}{\kappa}\ln\left(\frac{z(1)u_*}{\nu}\right) + B, \tag{12}$$

where $\langle|\boldsymbol{u}|\rangle(1)$ is the plane averaged horizontal velocity magnitude evaluated at $z(1)$, the first gridpoint away from the wall, and we have used $\kappa = 0.41$ and $B = 5.2$. Once the friction velocity is obtained, the components of the plane-averaged wall stress are estimated by specifying the angle $\alpha_0$ between the wall-stress and the $x$-direction:

$$\langle\tau\rangle_{13} = \rho_0 u_*^2 \cos(\alpha_0), \tag{13}$$

$$\langle\tau\rangle_{23} = \rho_0 u_*^2 \sin(\alpha_0). \tag{14}$$

The surface stress angle $\alpha_0$ is estimated using the finite Reynolds number theory of Spalart (1989) which gives $\alpha_0 = 20.6°$. The local wall stress is then estimated using fluctuations in the resolved horizontal velocity at the first gridpoint

$$\tau_{13}(x,y) = \frac{u(x,y,1)}{\langle u\rangle(1)}\langle\tau\rangle_{13}, \tag{15}$$

$$\tau_{23}(x,y) = \max\left(\frac{v(x,y,1)}{\langle u\rangle(1)}\langle\tau\rangle_{13}, \frac{v(x,y,1)}{\langle v\rangle(1)}\langle\tau\rangle_{23}\right). \tag{16}$$

The latter relation allows a smooth transition between the non-rotating case when the wall stress is dominated by the $\tau_{13}$ component and an Ekman layer where the mean velocity and wall stress in the spanwise direction are non-zero.

When applying the NWM–LES with low vertical resolution, spurious grid oscillations can arise in the wall-normal direction. In order to prevent this, a low-pass filter is applied to the velocity field in the vertical direction after each simulation time-step. A fourth-order compact filter is used for this purpose with the filter width parameter $\alpha = 0.48$ (Lele, 1992) which gives a very sharp transfer function so that only the highest wavenumbers are removed.

We have initialized each simulation with a steady-state temperature and velocity field from the large eddy simulations of Taylor and Sarkar (2007a). The temperature and velocity were interpolated onto the appropriate grid for the DNS, resolved LES, and NWM–LES. Steady state fields have been used in order to focus on the characteristics of a fully-developed boundary layer as opposed to the boundary layer formation. Each simulation was continued for about $t = 3/f$ non-dimensional time units which corresponds to about 8 h at a latitude of 45°. Unless otherwise noted, a Reynolds average, denoted by $\langle\cdot\rangle$ will be taken over horizontal planes and from $tf = 1.5$–3. Since the lower wall is adiabatic but a uniform heat flux is present in the outer layer, the thermal field does not reach a fully steady state, and the mixed layer depth increases gradually in time. In order to prevent smearing of the thin thermocline that forms above the mixed layer, the thermal profiles will not be averaged in time.

## 4. Results

### 4.1. Velocity structure

Before examining the performance of the LES in simulating the thermal structure of the boundary layer, it is useful to examine the mean velocity profiles. In constructing the wall model for the NWM–LES, we have made the assumption that the stratified and unstratified simulations obey the same logarithmic law. Since gridpoints near the wall are within the well-mixed layer, this seems reasonable, but it should be confirmed using the DNS. Fig. 3 shows the vertical shear normalized by the expected shear in the log-region:

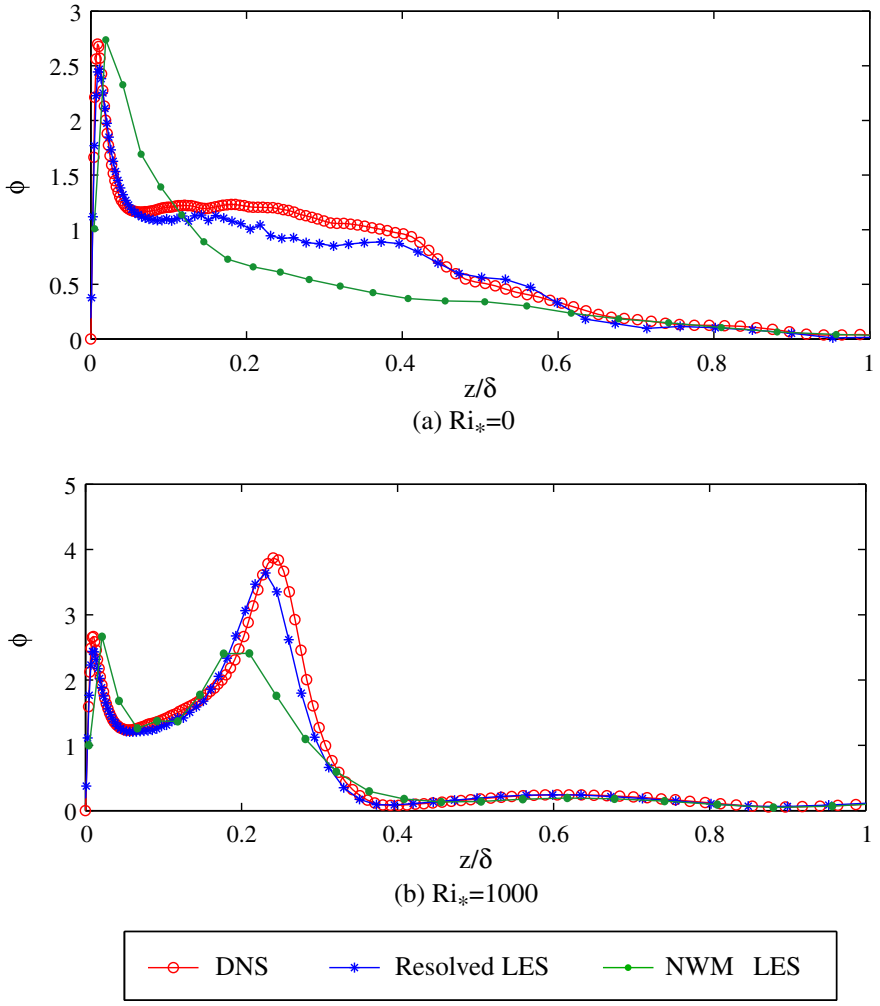


Fig. 3. Nondimensional shear, $\phi$ defined in Eq. (17).

$$\phi = \frac{\kappa z}{u_*}\left(\frac{\mathrm{d}\langle u\rangle}{\mathrm{d}z}^2 + \frac{\mathrm{d}\langle v\rangle}{\mathrm{d}z}^2\right)^{1/2}. \tag{17}$$

Based on this definition, when $\phi = 1$ the mean shear is in agreement with the expected value from the logarithmic law. As seen in Fig. 3a, the mean shear in the unstratified DNS follows the logarithmic law scaling for approximately $0.05 \leqslant z/\delta \leqslant 0.4$ and the resolved LES and to a lesser extent the NWM–LES are able to reproduce this profile. It may be possible to improve the representation of the mean velocity profile in NWM–LES using the adaptive stochastic forcing technique described by Taylor and Sarkar (2007b).

Fig. 3b shows that there is a small region, $0.05 < z/\delta < 0.1$, where the stratified Ekman layer also has $\phi \approx 1$. Therefore, the assumed form of the near-wall model is reasonable. It is also evident that the mean shear increases dramatically in the thermocline when $Ri^* = 1000$. The resolved LES is able to capture this increase, but the NWM–LES does not fully capture the maximum shear. This is not surprising since, as we will see, the NWM–LES also underestimates the temperature gradient in the thermocline.

The individual components of the mean horizontal velocity are shown in a hodograph in Fig. 4. As has been observed for an Ekman layer with a stabilizing surface heat flux, the presence of an outer layer stratification acts to increase the cross-stream velocity. This can be seen by comparing Fig. 4a and b. It is interesting to note that the angle of the Ekman spiral increases near the wall where the mean temperature gradient is zero. Therefore, the effect of stratification in this region appears to be non-local. The agreement between the resolved LES and DNS is excellent, while the NWM–LES over-estimates the cross-stream velocity in the unstratified simulation.

A useful definition for the height of a turbulent Ekman layer is the location where the streamwise Reynolds stress reaches 10% of its maximum value (Taylor and Sarkar, 2008). The boundary layer height, defined using this criteria, is shown in Fig. 5. One of the primary effects of the outer layer stratification is to decrease the Ekman layer height, as seen in this Figure. Both the resolved and NWM–LES capture the decrease in the boundary layer height reasonably well, although this is slightly overestimated in the resolved LES. The NWM–LES underestimates the

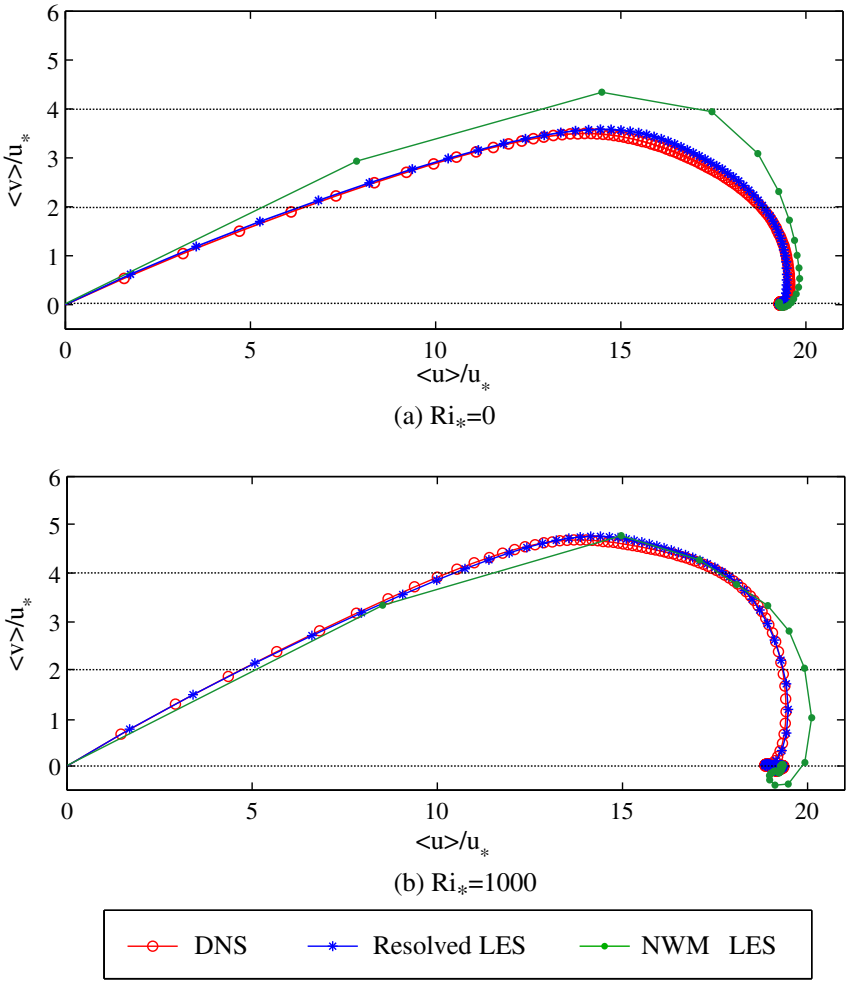


Fig. 4. Hodograph of the mean velocity.

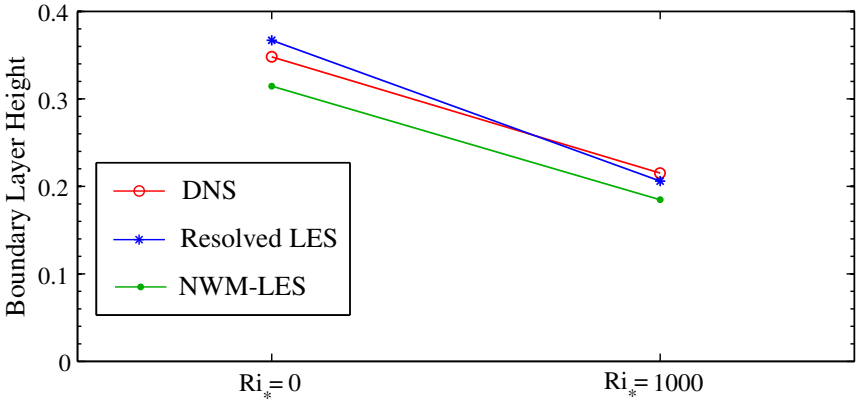


Fig. 5. Boundary layer height normalized by $\delta$, and defined as the location where the streamwise Reynolds stress, $\langle u'w' \rangle$, is 10% of its maximum value.

boundary layer height, both with and without an external stratification.

### 4.2. Thermal field

Since the lower wall is adiabatic and the molecular diffusion of heat is small compared to the turbulent flux, the heat content in the boundary layer is approximately conserved. In addition, at some location far enough from the boundary layer, the mean temperature profile is unchanged from its initial state. As a result, when the temperature profile mixes near the wall, the temperature gradient must increase above the mixed layer in order to return the temperature to the initial state. When the flow is

strongly stratified, the region with a non-zero turbulent heat flux is limited by stratification. In this case, the temperature gradient is large in a thermocline above the mixed layer. The mean temperature field in the stratified boundary layer can then be characterized by a three-layer structure with a well-mixed region near the wall, a strongly stratified thermocline, and an outer layer were the temperature gradient is equal to the initial value. This structure can be seen in the plane-averaged temperature gradient at $t = 3/f$, shown in Fig. 6b.

When $Ri^* = 0$, we still consider a uniform temperature gradient in the outer layer, but since the thermal and momentum equations become decoupled, the temperature is advected as a passive scalar. This allows us to evaluate the ability of the LES model to simulate both passive and active scalar mixing. The temperature profiles in both the resolved and NWM–LES compare well with the DNS when $Ri^* = 0$. Comparing Fig. 6a and b, it is evident that the mixed layer thickness is much smaller when $Ri^* = 1000$. In this case the mixed layer growth and the temperature gradient in the thermocline are under-predicted by the NWM–LES, and to a lesser extent by the resolved LES. When $Ri^* = 0$ the large eddies on the scale of the Ekman layer height are able to stir the temperature field since they are unaffected by the fluid density. Since there are relatively few of these large eddies in the domain, the instantaneous plane averaged temperature gradient shows more statistical noise when $Ri^* = 0$.

An important difference between the DNS and LES results is that both the resolved LES and the NWM–LES underestimate the rate of entrainment of outer layer fluid into the mixed layer. This can be quantified by comparing the rate of increase of the temperature of the mixed layer fluid. When the flow is strongly stratified and $Ri^* = 1000$, the rate of change of the mixed layer temperature is significantly underestimated in the LES. Specifically, $\mathrm{d}<\theta>/\mathrm{d}t$ in the mixed layer is $4.3 \times 10^{-3}$, $3.3 \times 10^{-3}$, and $2.1 \times 10^{-3}$, in the DNS, resolved LES, and NWM–LES, respectively, in units of $\mathrm{d}\langle\theta\rangle/\mathrm{d}z|_\infty \delta f$. When $Ri^* = 0$ and temperature acts as a passive scalar, the LES entrainment rate is in better agreement with the DNS.

The evolution of the mean temperature field can be written in terms of the molecular and turbulent heat flux:

$$\frac{\partial\langle\theta\rangle}{\partial t} = \frac{\partial}{\partial z}\left(\kappa\frac{\partial\langle\theta\rangle}{\partial z} - \langle\theta' w'\rangle\right). \tag{18}$$

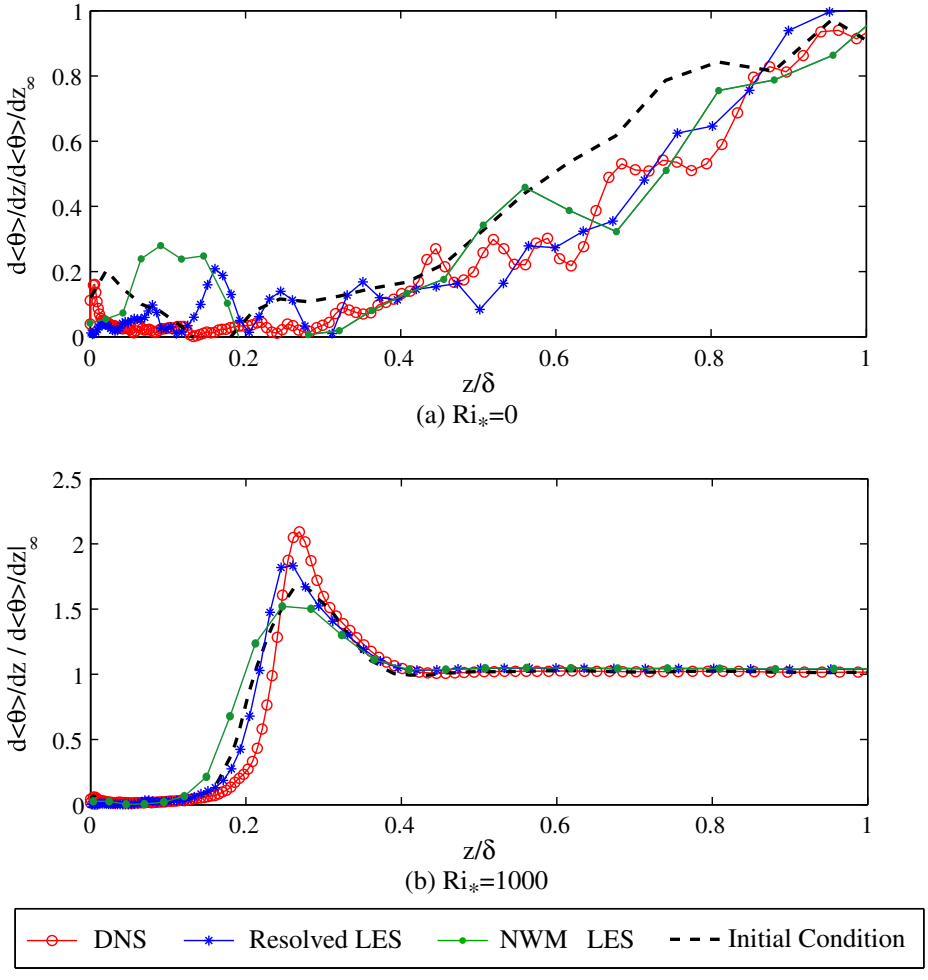


Fig. 6. Plane-averaged temperature gradient normalized by the outer value, evaluated at $t = 3/f$.

The right-hand side of Eq. (18) is dominated by the turbulent heat flux in the mixed layer and by the molecular heat flux above the thermocline. Since the heating of the mixed layer fluid is under-predicted by each LES when $Ri^* = 1000$, it follows that the estimate of the turbulent heat flux is also low. This is verified in Fig. 7. In both cases, the subgrid-scale contribution is shown by a dashed line. When $Ri^* = 0$ nearly all of the heat flux is accounted for by the resolved scales, while the subgrid-scale heat flux is more significant when $Ri^* = 1000$, particularly in the lower

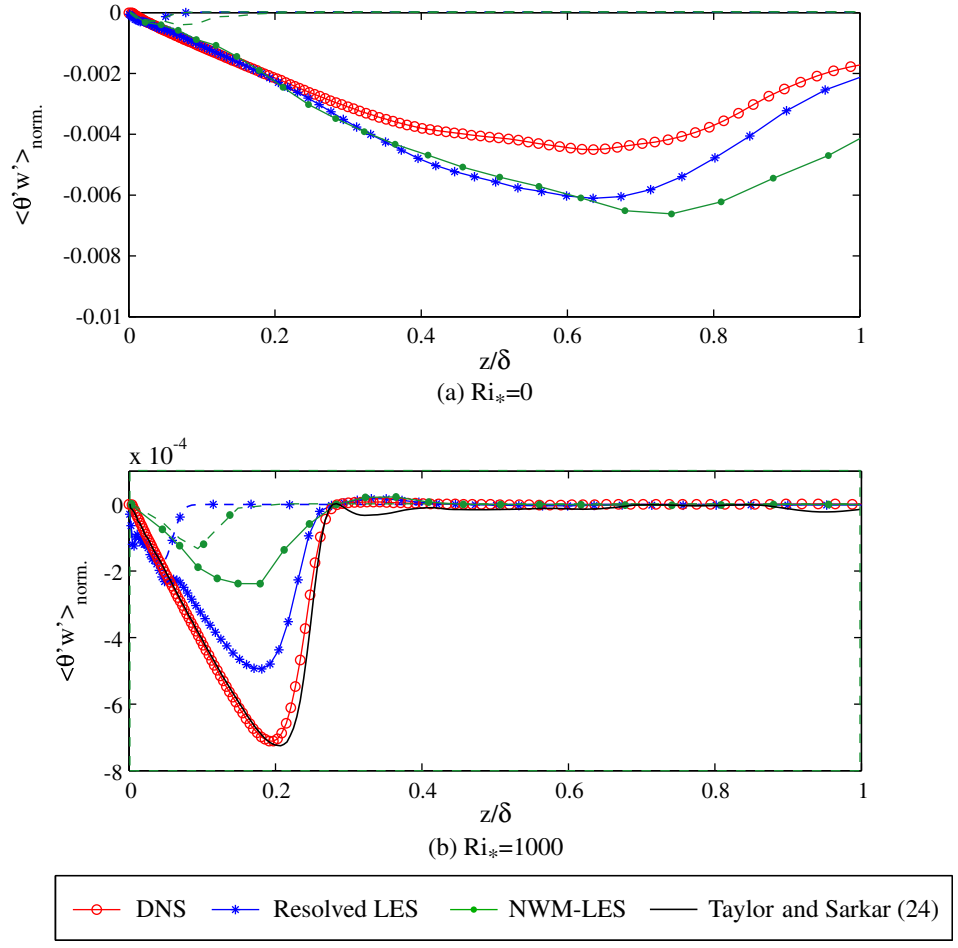


Fig. 7. Turbulent heat flux normalized by $\mathrm{d}\langle\theta\rangle/\mathrm{d}z|_\infty \delta u^*$. Solid lines show the total heat flux, dashed lines show the subgrid-scale contribution.

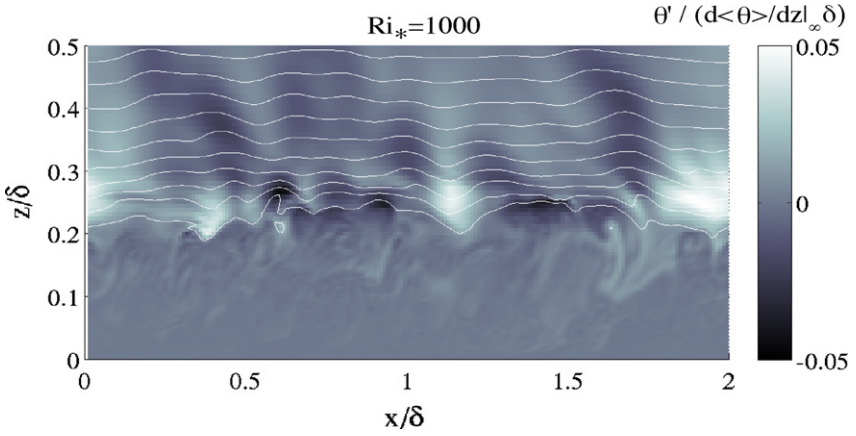


Fig. 8. Instantaneous visualization of the temperature field from DNS with $Ri^* = 1000$. Perturbations from the plane mean are shown in shades of gray, and white lines indicate isotherms.

half of the mixed layer. The curve in Fig. 7b from Taylor and Sarkar (2008) will be discussed in the conclusions section.

A visualization of the temperature field from the DNS with $Ri^* = 1000$ is shown in Fig. 8. In the mixed layer, small-scale overturns and filaments are visible. For comparison, at $z = 0.2\delta$ the vertical grid spacing in the DNS, resolved LES, and NWM–LES is $0.0058\delta$, $0.012\delta$, and $0.034\delta$, respectively. Since the vertical grid spacing in the NWM–LES at the top of the mixed layer is quite large, many of the small-scale features that are visible will not be resolved. Outside of the mixed layer, however, the

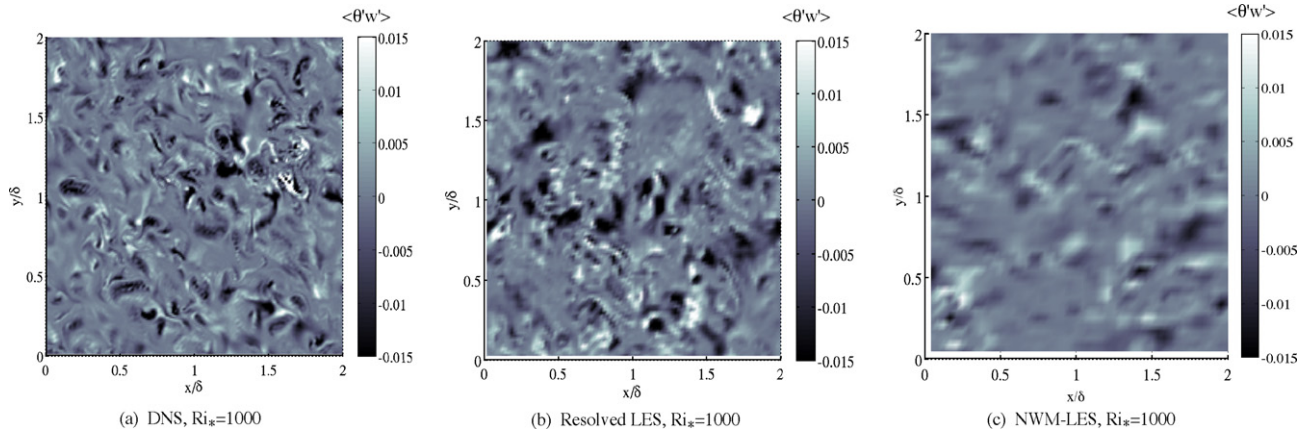


Fig. 9. Instantaneous visualization of the turbulent heat flux at $z/\delta = 0.2$, $Ri^* = 1000$.

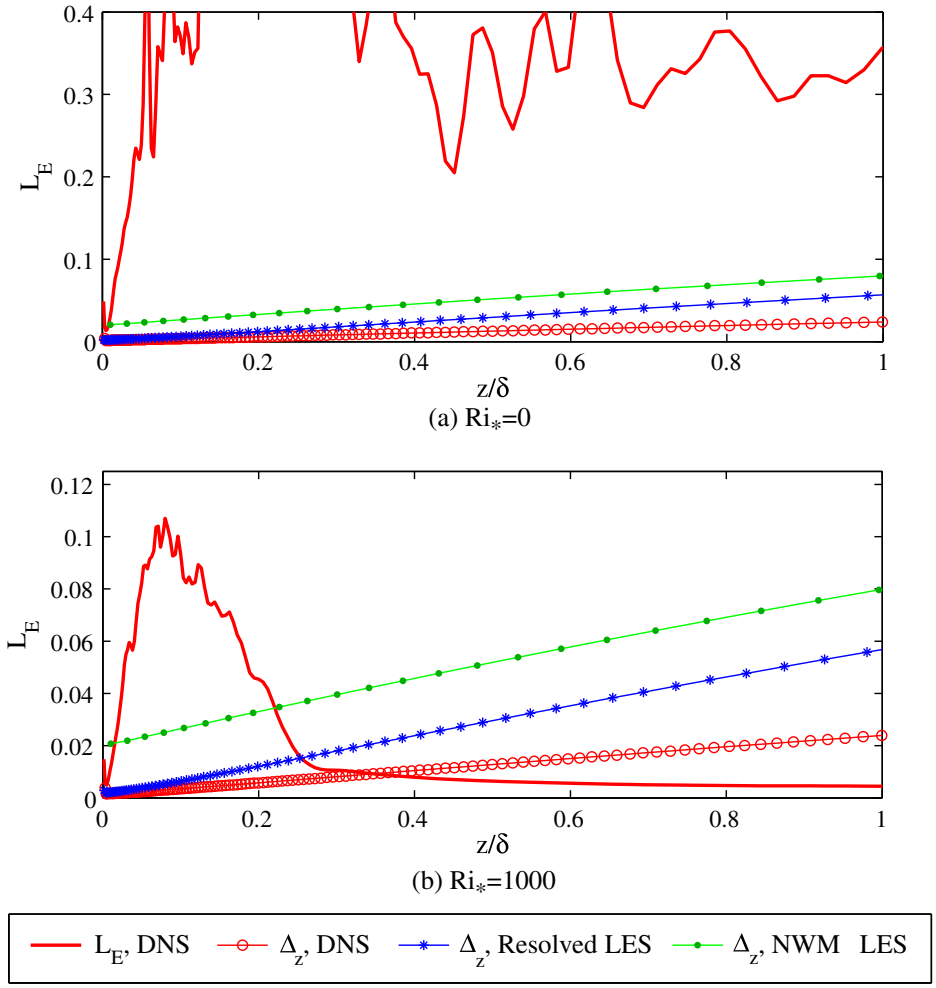


Fig. 10. Vertical grid spacing and Ellison scale.

characteristic scale of the temperature fluctuations increases dramatically. In the outer layer, stratification is strong enough to suppress turbulence, and temperature fluctuations are associated with internal wave field that is induced by eddies in the boundary layer. The properties of the internal wave field generated by a turbulent Ekman layer have been examined in detail by Taylor and Sarkar (2007a).

The horizontal scales in the $\langle\theta' w'\rangle$ field are visualized in Fig. 9 using a horizontal slice through $z = 0.2\delta$ (the location of maximum turbulent heat flux). At this location, $\langle\theta'^2\rangle$ and $\langle w'^2\rangle$ from the resolved and NWM–LES compare well with the DNS. As we have seen, however, the magnitude of $\langle\theta' w'\rangle$ is under-predicted by the LES. In Fig. 9, it is apparent that many of the small-scale features that are seen in the DNS are not present in the resolved or NWM–LES. Since the LES is unable to resolve all of the scales, and the subgrid-scale heat flux is negligible at this height, the plane averaged turbulent heat flux is underestimated.

Since the turbulent heat flux is significantly under-represented by the LES, it seems likely that small-scale motions contribute significantly to the turbulent heat flux at the top of the boundary layer. The length scale associated with density overturns can be estimated by the Ellison scale,

$$L_E = \frac{(\theta'^2)^{1/2}}{\mathrm{d}\langle\theta\rangle/\mathrm{d}z}. \tag{19}$$

The Ellison scale from the DNS, along with the vertical grid spacing in each simulation are shown in Fig. 10. When $Ri^* = 1000$, density stratification limits the scale of turbulent overturns, resulting in a much smaller Ellison scale compared to that when $Ri^* = 0$. In the DNS at $Ri^* = 1000$, at $z = 0.2\delta$, the Ellison scale is $L_E \simeq 0.03\delta$. At this location, the gridspacing in the NWM–LES is $(\Delta_x, \Delta_y, \Delta_z) = (0.04\delta, 0.04\delta, 0.03\delta)$ which clearly is not sufficiently to resolve the density overturns. The gridspacing in the resolved LES, at the same location, is roughly half of the Ellison scale. Therefore, the resolved LES is also not able to fully capture turbulent eddies at the Ellison scale, and underestimates the turbulent heat flux (see Fig. 7).

The turbulent Prandtl number, defined as the ratio of the turbulent viscosity and diffusivity can be written:

$$Pr_T = \frac{\nu_T}{\kappa_T} = \frac{\left(\langle u'w'\rangle^2 + \langle v'w'\rangle^2\right)^{1/2}}{-\langle\theta' w'\rangle} \frac{\mathrm{d}\langle\theta\rangle/\mathrm{d}z}{\mathrm{d}\langle|\mathbf{u}|\rangle/\mathrm{d}z}. \tag{20}$$

In both the stratified and unstratified DNS, the mixed region is characterized by $Pr_T \approx 1$ as has been previously re-

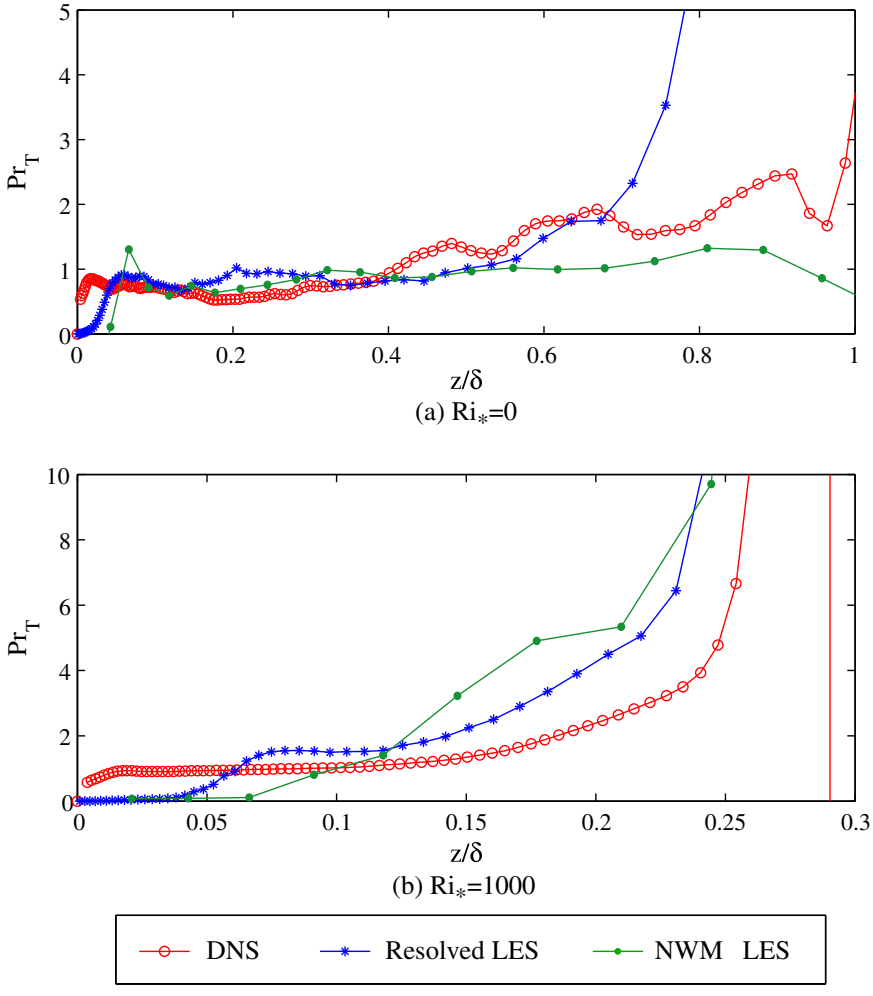


Fig. 11. Turbulent Prandtl number.

ported for turbulence in a low stratification environment (Schumann and Gerz, 1995). The low value of the turbulent Prandtl number near the wall in the LES is directly related to an underestimate of the mean temperature gradient. In the DNS, the temperature gradient only vanishes in a thin viscous layer near the wall. In each LES, the temperature gradient is much smaller near the wall. Specifically, at $z/\delta = 0.05$ when $Ri^* = 1000$, the temperature gradient normalized by the outer layer value is 0.0136, 0.0029, and 0.00094 in the DNS, resolved LES, and NWM–LES, respectively (see Fig. 11).

## 5. Conclusions

We have conducted simulations of an Ekman layer formed when a steady, linearly stratified fluid flows over a smooth boundary in the absence of a surface heat flux. The boundary layer thickness is strongly limited by the outer layer density stratification. A DNS was used to evaluate LES at two different resolutions with emphasis placed on the thermal structure of the boundary layer. We have found that when the temperature is treated as a passive scalar, both low and high resolution LES compare well with the DNS. However, when the outer layer is stratified, the turbulent heat flux in the boundary layer is significantly under-predicted by the LES. Flow visualizations revealed that small-scale motions that are not resolved by the LES, nor represented in the subgrid-scale model, are responsible for the entrainment of fluid into the boundary layer in the DNS. The Ellison scale provides a good estimate for the turbulent scales responsible for the entrainment and indicates that the entrainment motions are much smaller when the flow is stably stratified.

The dynamic mixed model used for the subgrid-scale terms does not adequately capture the subgrid-scale turbulent heat flux at the top of the mixed layer. One solution to this problem is to increase the resolution in the LES so that the Ellison scale, $L_E = \sqrt{\langle\theta'^2\rangle}/\mathrm{d}\langle\theta\rangle/\mathrm{d}z$, is resolved. Since the Ellison scale does not scale with the Reynolds number, and since the LES captures the mean velocity profile and the boundary layer height well, it is still possible to use this subgrid-scale model for a high Reynolds number LES. The overturning scale at the top of the mixed layer is limited by the potential energy needed to entrain the relatively light fluid from the pycnocline into the mixed layer. This scale can therefore be expected to scale with the Richardson number but not the Reynolds number of the flow. A NWM–LES with a dynamic Smagorinsky model was used by Taylor and Sarkar (2008) to simulate a stratified bottom Ekman layer at a field-scale Reynolds number of about $Re^* = 100{,}000$ with $N_x,N_y,N_z = 96,96,201$ gridpoints. The vertical resolution of these simulations in terms of the Ellison scale (not the Kolmogorov scale) was equivalent to that from the present DNS shown in Fig. 10. The turbulent heat flux from the simulation of Taylor and Sarkar (2008) with $Ri^* = 1000$ is included in Fig. 7. Despite the fact that the Reynolds number is much larger, the turbulent heat flux from these simulations shows excellent agreement with the DNS at the same Richardson number.

Thus far, we have considered non-dimensional quantities. It is useful to estimate relevant dimensional parameters for a typical oceanic bottom boundary layer. If the free stream velocity is taken to be $U_\infty = 5$ cm/s and with $u^*/U_\infty = 0.05$, $f = 10^{-4}\ \mathrm{s}^{-1}$, and $\nu = 10^{-6}\ \mathrm{m}^2/\mathrm{s}$, then $\delta = 25$ m and $Re^* = 62{,}500$. Clearly this Reynolds number is much larger than what we have considered here. Since $u^*/U_\infty$ does not depend strongly on the Reynolds number, if we keep the viscosity and the Coriolis parameter constant, $Re^* = 960$ is equivalent to a free stream velocity of $U_\infty = 0.077$ cm/s. The Richardson number $Ri^* = 1000$ implies that $N/f = 31.6$ so that the free stream buoyancy frequency is 1.86 cycles/h. With a thermal expansion coefficient of $\alpha = 10^{-4}\ ^\circ\mathrm{C}^{-1}$, this implies that the background temperature gradient is 0.01 °C/m. Although this temperature gradient is much smaller than is typically seen in engineering flows, buoyancy effects are still very important since the length scales are typically much larger in geophysical flows. In the deep ocean, buoyancy effects are significant since the velocities tend to be very low while the dynamical length-scales are large.

## References


Armenio, V., Sarkar, S., 2002. An investigation of stably stratified turbulent channel flow using large-eddy simulation. J. Fluid Mech. 459, 1–42.

Bewely, T., 1999. Optimal and robust control and estimation of transition, convection, and turbulence, Ph.D. thesis, Stanford University.

Bewely, T., 2007. Numerical methods for simulation, optimization, and control.

Businger, J., Charnock, H., 1983. Boundary layer structure in relation to larger scale flow: some remarks on the JASIN observations. Phil. Trans. R. Soc. Lond. A 308, 445–449.

Coleman, G., Ferziger, J., Spalart, P., 1992. Direct simulation of the stably stratified turbulent ekman layer. J. Fluid Mech. 244, 677–712.

Grant, A., 1992. The structure of turbulence in the near-neutral atmospheric boundary layer. J. Atmos. Sci. 49 (3), 226–239.

Grotzbach, G., 1987. Direct numerical and large eddy simulation of turbulent channel flows. In: Cheremisinoff, N. (Ed.), Encyclopedia of Fluid Mechanics, vol. 6. Gulf Publ., West Orange, NJ, pp. 1337–1391.

Klemp, J., Durran, D., 1983. An upper boundary condition permitting internal gravity wave radiation in numerical mesoscale models. Mon. Weather Rev. 111, 430–444.

Lele, S., 1992. Compact finite difference schemes with spectral-like resolution. J. Comp. Phys. 103 (1), 16–42.

Mahrt, L., 1999. Stratified atmospheric boundary layers. Boundary-Layer Meteorol. 90, 375–396.

Moin, P., Mahesh, K., 1998. Direct numerical simulation: a tool in turbulence research. Ann. Rev. Fluid Mech. 30, 539–578.

Orszag, S., 1971. Numerical simulation of incompressible flows within simple boundaries. 1. Galerkin (spectral) representation. Stud. Appl. Math. L, 293.

Piomelli, U., Ferziger, J., Moin, P., Kim, J., 1989. New approximate boundary conditions for large eddy simulations of wall-bounded flows. Phys. Fluids A 1 (6), 1061–1068.

Pope, S., 2000. Turbulent Flows. Cambridge University Press, Cambridge.

Schumann, U., 1975. Subgrid-scale model for finite difference simulation of turbulent flows in plane channels and annuli. J. Comp. Phys. 18, 376–404.

Schumann, U., Gerz, T., 1995. Turbulent mixing in stably stratified shear flows. J. Appl. Meteorol. 34, 33–48.

Shingai, K., Kawamura, H., 2002. Direct numerical simulation of turbulent heat transfer in the stably stratified ekman layer. Therm. Sci. Eng. 10, 25.

Spalart, P., 1989. Theoretical and numerical study of a three-dimensional turbulent boundary layer. J. Fluid Mech. 205, 319–340.

Taylor, J., Sarkar, S., 2007a. Internal gravity waves generated by a turbulent bottom Ekman layer. J. Fluid Mech. 590 (1), 331–354.

Taylor, J., Sarkar, S., 2007b. Near-wall modeling for LES of an oceanic bottom boundary layer. In: Proceedings of the Fifth International Symposium on Environmental Hydraulics.

Taylor, J., Sarkar, S., 2008. Stratification effects in a bottom Ekman layer. J. Phys. Oceanogr., submitted for publication.

Taylor, J., Sarkar, S., Armenio, V., 2005. Large eddy simulation of stably stratified open channel flow. Phys. Fluids 17, 116602.

Vreman, B., Geurts, B., Kuerten, H., 1997. Large-eddy simulation of the turbulent mixing layer. J. Fluid Mech. 339, 357–390.

Zang, Y., Street, R., Koseff, R., 1993. A dynamic mixed subgrid-scale model and its application to turbulent recirculating flows. Phys. Fluids A 5 (12), 3186–3196.

Zilitinkevich, S., Esau, I., 2003. The effect of baroclinicity on the equilibrium depth of neutral and stable planetary boundary layers. Q.J.R. Meteorol. Soc. 129, 3339–3356.